Eur. Phys. J. E **20**, 159–172 (2006)
DOI 10.1140/epje/i2006-10010-8

THE EUROPEAN PHYSICAL JOURNAL E

Collapse dynamics of smectic-A bubbles

F. Caillier[a] and P. Oswald[b]

Laboratoire de Physique de l'Ecole Normale Supérieure de Lyon, 46 Allée d'Italie, 69364 Lyon Cedex 07, France

Received 13 February 2006 and Received in final form 1 May 2006 /
Published online: 21 June 2006 –

Abstract. The collapse dynamics of smectic-A bubbles are analyzed experimentally and theoretically. Each bubble is expanded from a flat film stretched at the end of a hollow cylinder and deflated through a pressure release by means of a capillary tube. Its total collapse time can be varied between 0.1 s and 20 s by suitably choosing the length and the internal diameter of the capillary. This experiment allowed us to show that the collapse takes place in two steps: an initial one, which lasts a fraction of a second, where the meniscus destabilizes and fills up with focal conics, followed by a much longer period during which the bubble collapses and exchanges material with the meniscus. By measuring simultaneously the Laplace pressure and the internal pressure inside the bubble, we were able to fully characterize the shear-thinning behavior of the smectic phase within the meniscus. We emphasize that this method is generic and could be applied as well to other systems such as soap bubbles, on condition that inertial effects are negligible.

PACS. 47.55.dd Bubble dynamics – 83.80.Iz Emulsions and foams – 61.30.Jf Defects in liquid crystals

1 Introduction

Smectic films attracted attention for a long time. The reason is that they can be seen as model systems to study various problems such as confinement and surface effects on phase transitions, or membranes vibrations (for a review, see Chapt. 8 of Ref. [1]). The main reason is that films are mechanically very stable whatever their thickness $H = Nd$ (where N is the number of layers of thickness d). In practice, N can be varied between 3 and many thousands. The reason of this exceptional stability (for instance, with respect to usual soap films) is that a smectic film is made of elastic layers that can withstand the pressure difference imposed by the meniscus by which it is attached to its frame [2]. From this point of view, the film properties are indissociable from those of its meniscus which acts as a reservoir of material and fixes the pressure at rest in the whole system [3]. In spite of this stability, films of some materials can spontaneously thin when they are heated above their bulk transition temperature toward either the nematic phase (T_{AN}) [4, 2], or the isotropic liquid (T_{AI}) [5]. These transitions may be seen as phase transitions of a new type (for a review, see [6]). The thinning takes place by nucleation and growth of pores (which are usually loops of elementary edge dislocations) which slowly grow until they reach the meniscus surrounding the film. Note that one can also thin a film by one layer at lower temperature than T_{AN} or T_{AI} by artificially nucleating a pore with the aid of a thin heating wire placed under the film [7,8]. In all cases, the thinning is accompanied by dissipative processes which are mainly localized close to the core of the dislocation (characterized by its mobility m) and at the entrance of the meniscus in which the film material empties [1, 9]. In this particular region of the meniscus, the layers are well organized around elementary dislocations which are localized in the middle of the meniscus. This region distinguishes clearly from the rest of the meniscus which is strongly disorganized and full of focal conics [10] (Fig. 1). These domains are composed of ellipses and hyperbolae in focal position. They form a Grandjean-type wall close to the well-organized part of the meniscus [1].

It has been shown previously, first theoretically [1,9], that the flow around the dislocations contained in this well-oriented part of the meniscus is the principal source of dissipation. This mechanism was then evidenced experimentally, first by analyzing the slowing-down of pores when their diameter approaches that of the meniscus [11], and, second, by measuring the equilibration time of two menisci connected by a film [12]. In these two experiments, the velocities involved in the film around the core of the dislocations and at the entrance of the menisci were so small (of the order of μm/min or less) that it was possible to assume *linear relations* between the stress σ in the film and the dislocation velocity v ($v = m\sigma$, where m is the above-mentioned mobility), and between the pressure difference ΔP_{film} between the film and its meniscus and the material velocity v_m at the entrance of the meniscus

[a] e-mail: francois.caillier@ens-lyon.fr
[b] e-mail: Patrick.Oswald@ens-lyon.fr

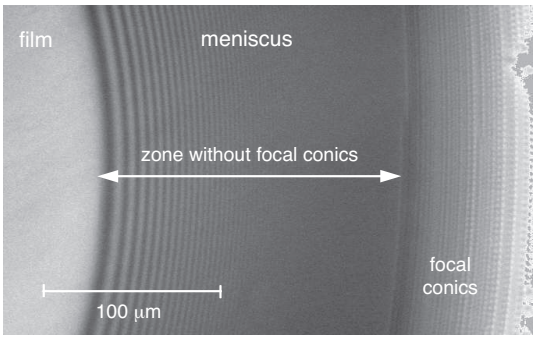

Fig. 1. Meniscus formed between a film and its frame (here a circular hole in a thin foil). One can discern the film on the left and the meniscus to the right. This photograph taken under combined lighting, both in reflection and in transmission, reveals that the meniscus is composed of a well-oriented zone (adjacent to the film) in which the only defects (invisible under the microscope) are elementary edge dislocations located in the middle of the meniscus, and of a zone full of focal conics (at the right edge, in the thickest region of the meniscus). When the film material enters into the meniscus, the dissipation takes place essentially in the well-oriented part of the meniscus.

($\Delta P_{film} = (C/m)v_m$). We recall that in this *quasi-static regime*, m is a constant, whereas the meniscus permeability C is a quantity that strongly depends on the film thickness $H = Nd$, where N is the number of layers in the film and d the layer thickness [1,9,11,12].

The question we address in this article is to determine what happens beyond the quasi-static regime, when velocities at the entrance of the meniscus are many orders of magnitude larger than in the previous experiments. This situation produces, for instance, each time a film is stretched on a frame. In this case, the film material is extracted at a large velocity from the meniscus which wets the frame. Unfortunately, this situation is difficult to analyze because the meniscus changes length and thus deforms continually.

Another way to process is to make a bubble from a flat smectic film which is stretched at the end of a hollow cylinder. In this experiment, the film is equilibrated until it has a constant thickness. Then, a bubble is slowly expanded by compressing the air inside the cylinder. The so-formed bubble is finally deflated through a thin capillary tube. This experiment was already performed by one of us (PO) almost twenty years ago [13]. It provided us with a method to measure the film tension, which was then widely used and improved by Stannarius *et al.* [14–16] to measure and compare the film tensions of various compounds. The experiment also showed that the smectic dissipates energy when the bubble collapses. Nevertheless, measurements were not performed under well-controlled conditions. In addition, the explanation given at that time about the origin of the dissipation was inexact, due to our ignorance about the film structure at the free surfaces and the mechanisms of dislocation nucleation.

These are the reasons why we redid much more carefully this experiment, although in different conditions, and analyzed it in the light of our actual knowledge about films and their menisci.

The plan of the article is as follows. In Section 2, we describe the experimental setup and the way to make a bubble with a controlled thickness. In Section 3, we show that the meniscus destabilizes before the bubble collapses. Section 4 is devoted to theory. First, the two fundamental equations describing the coupled time evolution of the height of the bubble and the pressure inside are established. These equations are used to first explain the initial destabilization of the meniscus and then to calculate the collapse dynamics by assuming that the meniscus permeability is constant. These predictions are compared to experiments in Section 5. We show that the assumption of a constant permeability of the meniscus is no longer valid during a bubble collapse but must be replaced by a new rheological law taking into account the non-Newtonian behavior of the destructured meniscus. In addition, we show that this law can be determined experimentally by measuring the difference between the Laplace pressure (obtained from the shape of the bubble) and the pressure inside the bubble. The case of thin films, which usually thicken during the collapse, is described separately in Section 6. Concluding remarks are drawn in Section 7.

2 Experimental setup and bubble formation

A schematic representation of our setup is shown in Figure 2. A film of the liquid crystal 8CB (4n-octyl-4′-cyanobiphenyl, from Frinton Laboratories) is stretched at the end of a hollow cylinder. The latter is conic at its end with a sharp circular edge of radius $r = 0.5\,\mathrm{cm}$. This particular shape prevents the film from gliding inside the cylinder, because, if it be so, its surface area and its energy would increase. In addition, the film remains flat after stretching, which is important for the observations in reflecting microscopy. To prepare thick films, we used a flexible metal blade coated at one edge by a small amount of liquid crystal. Maintaining this plate tilted and in contact with the edge of the cylinder, the film is very slowly stretched over the hole. To move the plate smoothly, it is fixed to a translation stage driven by a continuous current motor whose speed is reduced by a gearbox. Experiments show that the slower is the stretching, the thicker is the film. Typically, half an hour is necessary to prepare a $10\,\mu\mathrm{m}$ thick film. Once the film is prepared, it is equilibrated for a few hours. During this time, the meniscus takes a regular shape and rearranges as in Figure 1. The interior of the cylinder is connected to a syringe which has a volume of 50 ml and is fixed on a syringe pump whose pumping rate can be varied between 1 and 150 ml/h. This system allows us to inflate the bubble very slowly, within typically 5 to 15 min, which corresponds to pumping rates between 1 and 3 ml/h. In this way, the film thickness and the structure of the meniscus do not change during the inflation phase [17]. Each bubble is then deflated through a plastic capillary tube, of length L ranging between 6 and 192 cm and of inner radius $a \simeq 0.04\,\mathrm{cm}$. This tube is connected with a home-made valve. Its function is to open

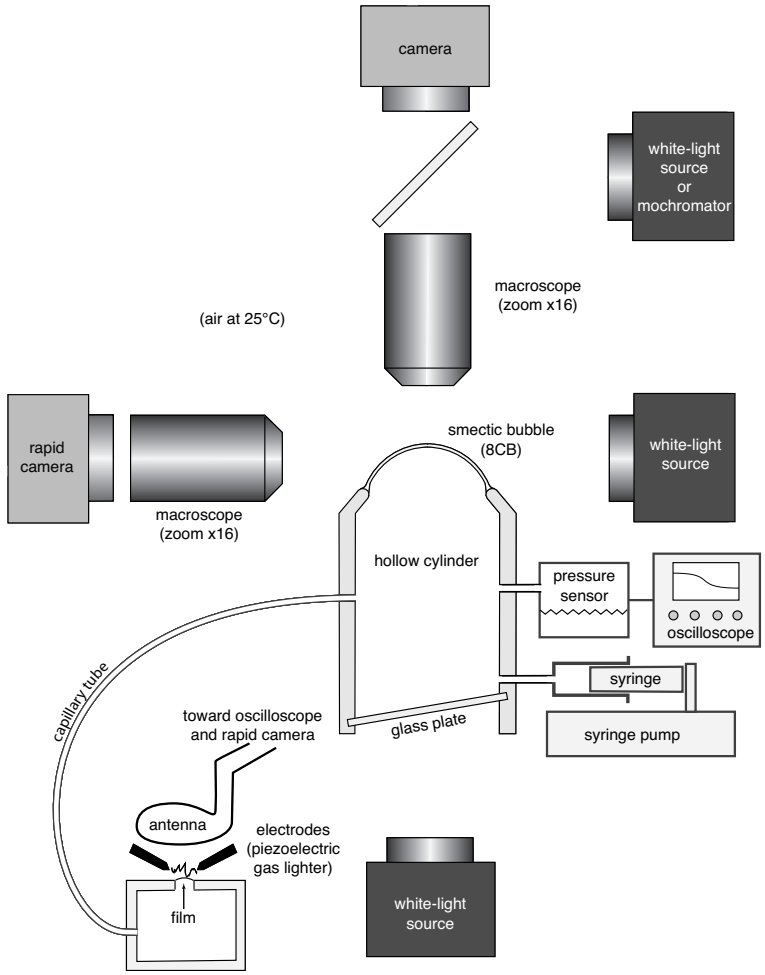

Fig. 2. Schematic of the experimental setup.

in due time the system initially closed as fast as possible without introducing perturbations. To fulfill these conditions, we used a small box with two holes: the first one is connected to the capillary tube, while the other, of 3 mm in diameter, is closed by a smectic film. Two electrodes placed above the film are plugged into a piezoelectric gas lighter. Activating the latter produces an electric spark which breaks the film and opens the system to the atmospheric pressure. By filming with a rapid camera the film rupture, we verified that the opening time is of the order of 0.25 ms (see Fig. 3). Two Leica macroscopes are used to visualize the bubble. One of them has its optical axis vertical and can work either by transmission or by reflection. This macroscope is equipped with a Panasonic video camera and with a $\times 16$ zoom objective which allows us to observe a part or the totality of the film. A white-light source and a monochromator are used to visualize the film and to measure its thickness by reflectivity (for more details see [1]). The optical axis of the second macroscope is horizontal. This macroscope works only in transmission. It is equipped with a white-light source and with a ultra-rapid video camera (Photron Fastcam Ultima 1024) which allows us to capture up to 4000 images/s with a resolution of 512×128 pixels.

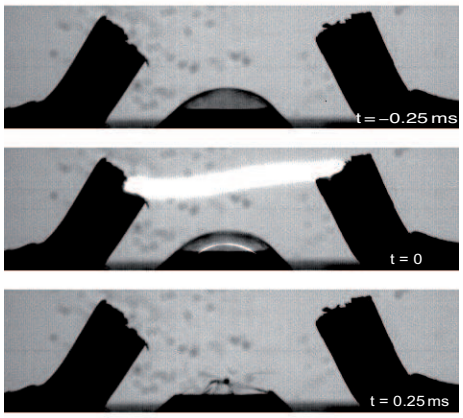

Fig. 3. Three photographs showing the opening of the smectic valve taken with the rapid camera. One sees that the film breaks within about 0.25 ms. Time marked on each frame is given by the internal timer of the rapid camera.

The images of the bubble (see Fig. 4) are then analyzed on a PC computer with Igor Pro software (Wavemetrics, Lake Oswego, OR). A program automatically detects the bubble profile and then calculates its radius of curvature,

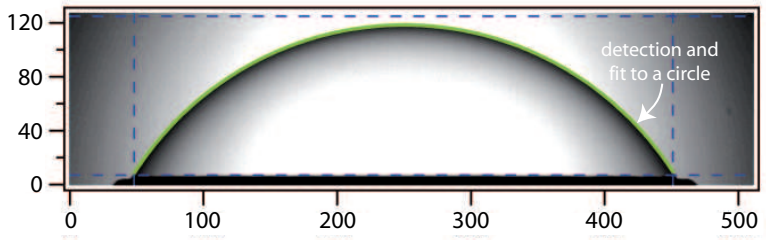

Fig. 4. Photograph of a bubble taken with the "horizontal" macroscope. The program of image processing first determines the zone of interest (inside the rectangle in dashed line). The edge of the bubble is then detected and fitted to a circle whose radius R and center coordinates (x_0, y_0) are measured. In this example, (where the dimensions are given in pixels), the program gives $R = 240.2$, $x_0 = 249.9$ and $y_0 = -121.8$.

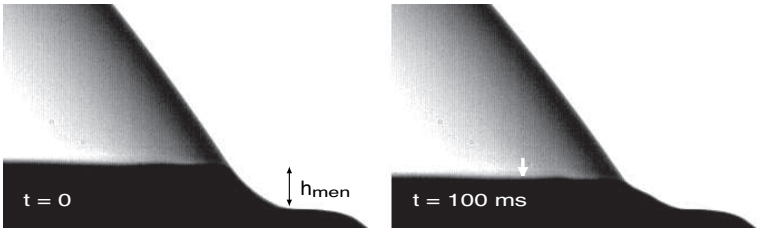

Fig. 5. Two side views of the bubble and its meniscus taken at 100 ms interval with the rapid camera. One sees that the radius of curvature of the bubble has not changed. On the other hand, the meniscus (which is black under these illumination conditions) has clearly changed height.

the coordinates of its center, and its height above the rim of the cylinder. A low differential pressure sensor Druck LPM5480 is used to measure the pressure inside the bubble. This sensor works in the range ±50 Pa with an accuracy better than ±0.25% and has a response time of 10 ms. Its analog output (±5 V) is connected to a deep-memory digital oscilloscope Agilent 54621 which records the pressure curve during the collapse. Finally, an antenna, simply consisting of an electrical wire forming a loop, is connected to the external trigger input of the oscilloscope. Experiments show that the voltage produced at the terminals of the antenna varies by about 5 V over less than one μs, which is largely enough to trigger the oscilloscope. In parallel, the rapid camera is triggered by the output signal of the oscilloscope. This piezoelectric smectic valve coupled with the antenna allows us to trigger and synchronize with a remarkable accuracy (within a few μs) the pressure and profile measurements. Note that this system was used to film the spark and the valve opening shown in Figure 3. In this example, the capture frequency of the camera was set to 4000 images/s. The fact that the spark is visible in the photograph corresponding to time $t = 0$ of the internal timer of the camera demonstrates the good functioning of our synchronization system.

3 Meniscus destabilization and collapse dynamics of the bubble: experimental results

The collapse dynamics of a smectic bubble decomposes into two steps.

The first step is very short and essentially consists of a destructuration of the meniscus.

The second step is much longer and corresponds to the collapse itself during which the film penetrates into the meniscus.

The experiment shown in this section (as all the others described in this article) was performed at room temperature (25 ± 0.5 °C). The film thickness, measured by reflectivity, was 1840 (in number of layers N). The bubble was inflated very slowly in order that the film keeps a constant thickness. To study the collapse dynamics, we simultaneously recorded the pressure inside the bubble and the bubble profile from which the radius of curvature was deduced by image processing. For some practical reasons which will appear clearly in the following, the bubble was expanded by half, so that its initial height x above the rim of the cylinder was equal to $x_0 = r/2 = 0.25$ cm. The bubble was then deflated through a 6 cm long capillary tube.

3.1 Meniscus destabilization

Observations immediately after the valve opening of the whole bubble show that it does not change shape, but instead settles down due to the meniscus receding. This is well visible in Figure 5, where we focused on the meniscus.

From the photographs taken with the horizontal-axis macroscope and the rapid camera, the height of the meniscus h_{men} and the radius of curvature R of the bubble were measured as a function of time. This second measurement allowed us to calculate the Laplace pressure $\Delta P_L = 4\gamma/R$, where γ is the smectic-air surface tension. Note that ΔP_L represents the difference with the atmospheric pressure which would be measured on condition that the bubble is at equilibrium. In the dynamical regime, this quantity is different from the real pressure ΔP_i which is measured

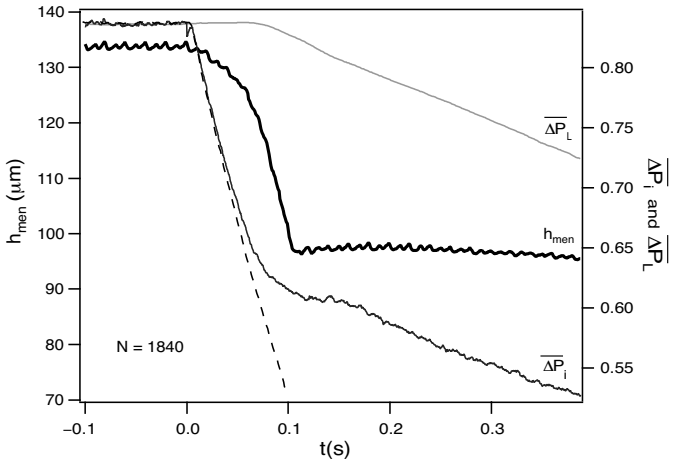

Fig. 6. Analysis of the meniscus receding: time evolution of the meniscus height h_{men} and of the two dimensionless pressure differences, $\overline{\Delta P}_i$ and $\overline{\Delta P}_L$ ($N = 1840$, $L = 6\,\mathrm{cm}$). The dashed line represents the $\overline{\Delta P}_i$ curve which is recorded when the smectic bubble is replaced by a rigid membrane.

inside the bubble (and is also referred to the atmospheric pressure).

In Figure 6, we plotted the three curves $h_{men}(t)$, $\overline{\Delta P}_i(t) = \Delta P_i(t)/\Delta P_{max}$ and $\overline{\Delta P}_L(t) = \Delta P_L(t)/\Delta P_{max}$ measured experimentally. Pressures are here normalized to the maximal pressure difference $\Delta P_{max} = 4\gamma/r$ (corresponding to a bubble at rest of radius of curvature $R = r$). We first note in the graph that before the valve opening, the internal pressure is equal to the Laplace pressure, as it must be in the static regime at equilibrium. The graph then clearly shows that during the first 100 ms, $\overline{\Delta P}_L$ remains unchanged, whereas h_{men} and $\overline{\Delta P}_i$ abruptly decrease. To complete these observations, we checked that during this period of time, $\overline{\Delta P}_i$ decreases in the same way as when the cylinder is closed with a solid membrane while the air inside is compressed at the same initial pressure as with the smectic bubble. This is compatible with our observations that the bubble behaves as a rigid spherical cap at the beginning of the process. To better understand what happens in this regime, we also recorded transmission images of the meniscus taken with the vertical-axis macroscope (Fig. 7). To see better the meniscus, we used the largest magnification as possible. The first picture at time $t = 0$ shows the meniscus at equilibrium. As already emphasized in the introduction, it is composed of a transparent well-organized zone and of a disorganized zone which strongly scatters light and, thus, appears darker than the other. This second zone is full of focal conics among which the biggest ones are discernible in the photographs. Observations of the meniscus during the first 100 ms show that its well-oriented part reduces in size and becomes unstable with respect to the formation of a lattice of focal parabolae [1,18]. These defects are clearly visible in the second photograph taken 100 ms later. This photograph marks the end of the first step of destabilization of the meniscus. It must be noted that during this time, the surface area of the film does not change, which implies that there is no exchange of material between the film and the meniscus which only recedes because of the destructuration of its well-oriented part. This first step of destabilization is followed by the collapse of the bubble which we now describe.

3.2 Collapse dynamics

The collapse really starts once the meniscus has been destabilized. The internal pressure $\overline{\Delta P}_i$ continues to decrease, but much more slowly than during the initial step of destabilization of the meniscus. In the same time, the Laplace pressure $\overline{\Delta P}_L$, initially constant and equal to $\overline{\Delta P}_i(t = 0)$, starts to decrease as $\overline{\Delta P}_i$. The two pressure curves are shown in Figure 8. They are clearly shifted, which is a direct evidence that the static Laplace law does no longer apply during the collapse. We also plotted in the same graph the relative pressure variation $\overline{\Delta P}_r = (\Delta P_L - \Delta P_i)/\Delta P_L$ whose physical meaning will be given in the next section. This quantity, which characterizes the shift to the Laplace law, starts from 0 at $t = 0$, abruptly increases, passes through a maximum when the meniscus destabilizes, and then decreases to finally tend to 0 at long time. Note that the curve $\overline{\Delta P}_r$ becomes noisy at long time as it is defined as the ratio between two quantities which tend to 0 in this limit.

4 Theoretical predictions

In this section, we establish the two fundamental equations that govern the collapse dynamics of a smectic bubble. Then, we shall use these equations to explain the meniscus instability and to predict the main characteristics of the collapse, in particular of the pressure curves.

4.1 The two fundamental laws

The first law relates the dissipation in the smectic phase Φ_{Sm} to both the variation of the film surface area $\mathrm{d}S/\mathrm{d}t$ and the shift to the static Laplace law $\overline{\Delta P}_r$. The second law is the Poiseuille law written by taking into account the air compressibility effects.

4.1.1 Relation between the smectic dissipation and the shift to the Laplace law

To obtain this equation, let us consider a closed system consisting of the smectic bubble (film + meniscus) and a constant volume of air contained in the bubble and a part of the cylinder (Fig. 9). Let S be the surface area of the bubble and V its volume.

The driving force of the collapse is the gain of surface energy $2\gamma \mathrm{d}S/\mathrm{d}t$, negative by convention. On the other hand, the energy lost by dissipation in the smectic phase (*i.e.*, in the film and the meniscus), Φ_{Sm}, is positive and

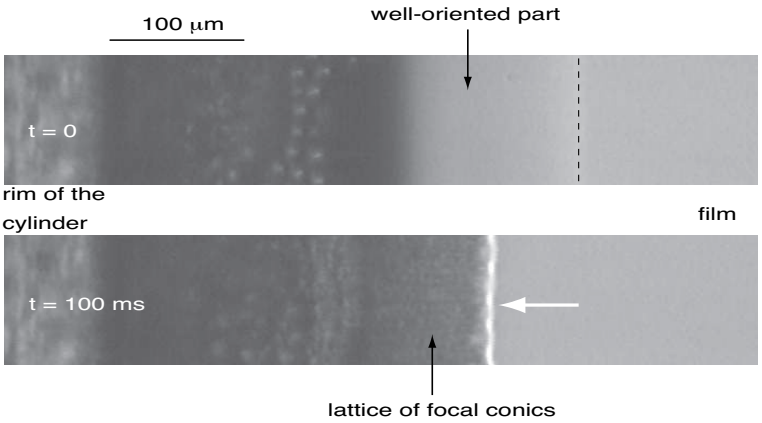

Fig. 7. Meniscus destructuration. These two transmission photographs have been taken with the vertical-axis microscope at the beginning ($t = 0$) and at the end ($t = 100\,\mathrm{ms}$) of the stage of the meniscus receding ($N = 1840$, $L = 6\,\mathrm{cm}$).

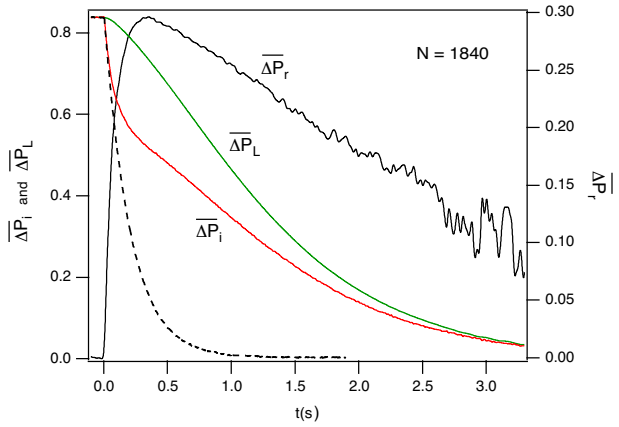

Fig. 8. Time evolution of the pressure inside the bubble, of the Laplace pressure deduced from the radius of curvature of the bubble, and of the relative pressure variation ($N = 1840$, $L = 6\,\mathrm{cm}$). The dashed line represents (as in Fig. 6) the $\overline{\Delta P_i}$ curve that is recorded when the smectic bubble is replaced by a rigid membrane.

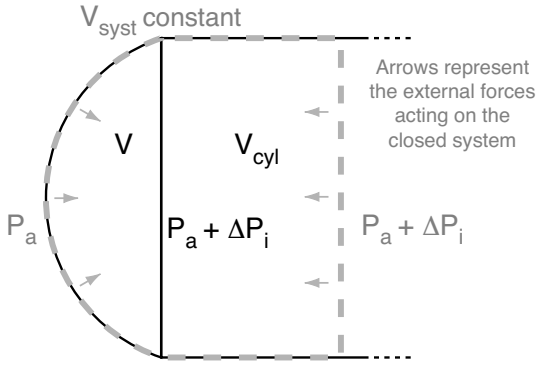

Fig. 9. The closed system chosen is delimited by the dashed line. It includes the film, the meniscus, and a constant volume of air contained in the bubble (of volume V) and in a part of the cylinder (of volume V_{cyl} such that $V_{syst} = V + V_{cyl} = \mathrm{const}$).

slows down the dynamics. The sum of these two terms represents the energy variation of the system. If the inertial effects can be neglected (which is indeed the case experimentally, as we shall show in the next subsubsection), this quantity is equal to the power of the external pressure forces that the system surfaces experience. There are two terms of this type. The first one, equal to $-P_a \mathrm{d}V/\mathrm{d}t$, is positive and represents the power of the atmospheric pressure forces acting on the surface of the bubble; the second, of expression $(P_a + \Delta P_i)\mathrm{d}V/\mathrm{d}t$, is negative and corresponds to the power of the internal pressure forces acting on the plane surface limiting the air volume inside the cylinder (see Fig. 9). Balancing all these terms, we obtain

$$2\gamma \frac{\mathrm{d}S}{\mathrm{d}t} - \Delta P_i \frac{\mathrm{d}V}{\mathrm{d}t} + \Phi_{Sm} = 0, \qquad (1)$$

where the atmospheric pressure has disappeared as it has been taken as reference. Due to the spherical geometry of the bubble, we have

$$\frac{\mathrm{d}S}{\mathrm{d}t} = \frac{2}{R}\frac{\mathrm{d}V}{\mathrm{d}t}, \qquad (2)$$

where R is the radius of curvature of the bubble. Substituting this relation into equation (1) gives

$$\left(\frac{4\gamma}{R} - \Delta P_i\right)\frac{\mathrm{d}V}{\mathrm{d}t} + \Phi_{Sm} = 0. \qquad (3)$$

This equation shows that the Laplace law is verified ($\Delta P_i = 4\gamma/R$) when the dissipation is negligible ($\Phi_{Sm} = 0$) and fails in a dissipative system. This can be seen also by introducing $\overline{\Delta P}_r$ into equation (1) which becomes with the aid of equation (2):

$$\Phi_{Sm} = \Delta P_i \frac{R}{2}\frac{\mathrm{d}S}{\mathrm{d}t} - 2\gamma \frac{\mathrm{d}S}{\mathrm{d}t} = 2\gamma \frac{\mathrm{d}S}{\mathrm{d}t}\overline{\Delta P}_r. \qquad (4)$$

A perhaps more enlightening way to rewrite this fundamental equation is to introduce the velocity v_m of the material at the entrance of the meniscus and the pressure difference between the film and the meniscus $\Delta P_{film} = P_N - P_m$, where P_N is the pressure inside the film and P_m

the pressure in the bulk of the meniscus. Indeed, if the film thickness remains unchanged during the collapse, the dissipation is essentially due to the flux of material at the entrance of the meniscus $2\pi r H v_m = -H\mathrm{d}S/\mathrm{d}t$, itself driven by ΔP_{film}. In these conditions, the dissipation reads

$$\Phi_{Sm} = -\Delta P_{film}\, H\, \frac{\mathrm{d}S}{\mathrm{d}t}\,. \tag{5}$$

Comparing this equation to equation (4), we obtain a relation between ΔP_{film} and $\overline{\Delta P}_r$:

$$\Delta P_{film} = -\overline{\Delta P}_r\, \frac{2\gamma}{H}\,. \tag{6}$$

This equation, as equation (4), shows that the shift to the Laplace law is really the pertinent quantity to characterize the dissipation inside the meniscus. We must also emphasize that all the equations written so far are general, provided that the film thickness remains constant during the collapse.

Nevertheless, we need to know the rheological behavior of the meniscus to solve explicitly the problem of the collapse dynamics. In the rest of this theoretical section, we shall assume, to simplify, that there exists, as in the quasi-static regime [1,11,12], a linear relation between ΔP_{film} and v_m:

$$\Delta P_{film} = \frac{C}{m}\, v_m, \tag{7}$$

where $v_m = -1/(2\pi r)\mathrm{d}S/\mathrm{d}t$. Under this assumption, we find from equation (5) a new expression for the dissipation:

$$\Phi_{Sm} = \frac{1}{2\pi r}\,\frac{CH}{m}\left(\frac{\mathrm{d}S}{\mathrm{d}t}\right)^2. \tag{8}$$

Finally, the fundamental equation (4) becomes by using the previous equation:

$$2\gamma\,\overline{\Delta P}_r = \frac{1}{2\pi r}\,\frac{CH}{m}\,\frac{\mathrm{d}S}{\mathrm{d}t}\,. \tag{9}$$

So measuring $\overline{\Delta P}_r$ and $\mathrm{d}S/\mathrm{d}t$ allows us, in principle, to determine the meniscus permeability C (or, more generally, the dissipation).

4.1.2 Poiseuille equation and compressibility effects

The second fundamental equation which governs the dynamics of the system is given by the classical Poiseuille law associated to the air flow in the capillary. In practice, many conditions must be fulfilled experimentally in order that this law is applicable, which we assume for the time being (for a discussion, see the end of this subsection). Let a be the internal radius of the capillary, L its length, η_a the dynamical air viscosity (which is pressure independent [19] as long as the air can be considered as a perfect gas) and Q_v the air volume flux through the capillary. The Poiseuille law reads

$$\Delta P_i = \frac{8\eta_a L}{\pi a^4}\, Q_v. \tag{10}$$

If the air was incompressible, we would have $Q_v = -\,\mathrm{d}V/\mathrm{d}t$. In reality, the air compressibility cannot be neglected as can be seen from the curve $\overline{\Delta P}_i(t)$ in dashed line in Figure 8 representing the pressure evolution in the system when it is closed by a solid membrane. Indeed, this curve would "instantaneously" jump to zero if the air was incompressible, which is not the case. To take into account the compressibility of the air contained in the bubble and the dead volume (inside the cylinder and the pressure sensor), let us first consider that the air behaves as a perfect gas at constant temperature. Let ρ_a be its density at the atmospheric pressure. When its pressure varies by ΔP_i, its density varies by $\delta\rho_a$ given by

$$\frac{\Delta P_i}{P_a} = \frac{\delta\rho_a}{\rho_a} \ll 1. \tag{11}$$

Let m_a be the mass of air inside the bubble (of volume V) and the cylinder together with the pressure sensor (of volume $V_{dead} \gg V$). We have

$$m_a = (\rho_a + \delta\rho_a)(V + V_{dead}) \tag{12}$$

from which we calculate, by using equation (11),

$$\frac{\mathrm{d}m_a}{\mathrm{d}t} \approx \rho_a\,\frac{\mathrm{d}V}{\mathrm{d}t} + V_{dead}\,\frac{\mathrm{d}\delta\rho_a}{\mathrm{d}t} = \rho_a\,\frac{\mathrm{d}V}{\mathrm{d}t} + \frac{V_{dead}}{P_a}\,\frac{\mathrm{d}\Delta P_i}{\mathrm{d}t}\,. \tag{13}$$

Dividing this equation by ρ_a yields

$$Q_v = \frac{\mathrm{d}V}{\mathrm{d}t} + \frac{V_{dead}}{P_a}\,\frac{\mathrm{d}\Delta P_i}{\mathrm{d}t}\,. \tag{14}$$

Finally, the second fundamental equation is obtained by replacing Q_v by its expression in equation (10):

$$\Delta P_i = \frac{8\eta_a L}{\pi a^4}\left(\frac{\mathrm{d}V}{\mathrm{d}t} + \frac{V_{dead}}{P_a}\,\frac{\mathrm{d}\Delta P_i}{\mathrm{d}t}\right). \tag{15}$$

Note that this equation still applies when the smectic bubble is replaced by a solid membrane. In this case, $\mathrm{d}V/\mathrm{d}t = 0$, which gives the simplified equation

$$\Delta P_i = \frac{8\eta_a L}{\pi a^4}\,\frac{V_{dead}}{P_a}\,\frac{\mathrm{d}\Delta P_i}{\mathrm{d}t}\,. \tag{16}$$

This equation predicts that the pressure decreases exponentially as a function of time, with the characteristic time

$$t_a = \frac{8\eta_a L}{\pi a^4}\,\frac{V_{dead}}{P_a}\,. \tag{17}$$

It turns out that the curve in dashed line in Figure 8 fits very well to an exponential law. From this fit, we deduced an experimental value of t_a of the order of 0.41 s for a capillary of length $L = 6$ cm. In addition, we checked experimentally that t_a is proportional to L. On the other hand, the volume V_{dead} we found from this measurement was typically 10 times larger than that estimated experimentally. It turns out that this discrepancy can be easily explained by taking into account the deformation of the flexible metallic membrane that serves to measure the

pressure inside the pressure sensor. More exactly, it can be proved [20] that the whole system behaves as if the dead volume was larger than the real one. For this reason, we shall continue to call V_{dead} this effective volume in the following.

Finally, let us mention that it can be shown (for more details, see ref. [20]) that the Poiseuille law applies. In particular, we have checked that in all experiments, the end effects are negligible (indeed, a certain distance is necessary to reach the parabolic velocity profile inside the capillary; in our experiments, this distance is always at least 100 times smaller than L). We also verified that all inertial effects due to the fact that the flow is not stationary during a collapse can be neglected. Two of them are due to the air. They are characterized by two typical inertial times: $t_{ia}^{cap} \sim \rho_a a^2/\eta_a$ which takes into account the inertia of air inside the capillary and $t_{ia}^{dead} \sim \sqrt{\rho_a V_{dead} r^3/V\gamma}$ which takes into account the inertia of air inside the dead volume (the true one!). Another time is associated to the film inertia: $t_i^{film} \sim r\sqrt{H\rho_{Sm}/\gamma}$. It can be verified that t_{ia}^{cap} and t_{ia}^{dead} are of the order of 10^{-2} s, while t_i^{film} is still shorter (10^{-3} s for $N = 500$). All these times are much smaller than all the typical times which are important in this problem (see the next subsubsection). So, we shall neglect them in the following. Finally, we checked that the Reynolds number associated to the air flow inside the capillary is always much smaller than the critical Reynolds number (of the order of 1000 [21]) above which the flow becomes turbulent.

4.1.3 Dimensionless equations and characteristic times

We have already defined time t_a characterizing the air compressibility (Eq. (17)). From the previous equations, we can construct two other important times. The first one, we shall call the *smectic time*, reads, according to equation (9),

$$t_{Sm} = \frac{CHr}{2\gamma m}\,. \tag{18}$$

It characterizes the dissipation at the entrance of the meniscus and contributes to the slowing-down of the collapse. When written in this form, this time is associated with the permeation flow around the cores of the dislocations as we assume that equation (7) applies.

The second time, named *capillary time*, has for expression, according to equation (15),

$$t_c = \frac{4}{3}\,\frac{\eta_a L r^4}{\gamma a^4} \tag{19}$$

and results from a balance between the surface tension forces in the bubble and the viscous forces in the capillary. This time fixes the typical duration of the collapse.

Note that time t_a can be rewritten as a function of time t_c in the form

$$t_a = \frac{8}{3}\,\frac{\Delta P_{max}}{P_a}\,\frac{V_{dead}}{V_{max}}\,t_c. \tag{20}$$

In the following, we set

$$\kappa = \frac{t_a}{t_c} \quad \text{and} \quad \xi = \frac{t_{Sm}}{t_c} \tag{21}$$

and we introduce the dimensionless quantities

$$\overline{\Delta P}_i = \frac{\Delta P_i}{\Delta P_{max}}, \quad \bar{t} = \frac{t}{t_c}, \quad \text{and} \quad \bar{x} = \frac{x}{r}\,, \tag{22}$$

where t is the time and x the height of the bubble with respect to the extremity of the cylinder. We also recall that for a spherical cap, we have

$$V = \frac{\pi}{6}\,x(x^2+3r^2), \quad S = \pi(x^2+r^2), \quad \text{and} \quad R = \frac{x^2+r^2}{2x}\,. \tag{23}$$

Using these relations, the two fundamental equations (9) and (15) rewrite in the following dimensionless forms:

$$\overline{\Delta P}_r = 1 - \frac{1+\bar{x}^2}{2\bar{x}}\,\overline{\Delta P}_i = -\xi\bar{x}\,\frac{\mathrm{d}\bar{x}}{\mathrm{d}\bar{t}}\,, \tag{24}$$

$$\overline{\Delta P}_i = -\kappa\,\frac{\mathrm{d}\overline{\Delta P}_i}{d\bar{t}} - 2(1+\bar{x}^2)\,\frac{\mathrm{d}\bar{x}}{\mathrm{d}\bar{t}}\,. \tag{25}$$

These two coupled equations in $\overline{\Delta P}_i$ and $\bar{x}$, together with the initial conditions

$$\bar{x}(\bar{t}=0) = \bar{x}_0 \quad \text{and} \quad \overline{\Delta P}_i(\bar{t}=0) = \frac{2\bar{x}_0}{1+\bar{x}_0^2} \tag{26}$$

determine the time evolution of the bubble during the collapse. Solving them numerically gives $\overline{\Delta P}_i(\bar{t})$ and $\bar{x}(\bar{t})$, from which we can deduce $\overline{\Delta P}_r(\bar{t})$.

4.1.4 Analytical results in the incompressible limit

It is very instructive to solve the problem in the incompressible limit ($\kappa = 0$). In this case, we obtain from equations (24) and (25), after elimination of $\overline{\Delta P}_i$,

$$\left[\frac{(1+\bar{x}^2)^2}{\bar{x}} + \xi\bar{x}\right]\frac{\mathrm{d}\bar{x}}{\mathrm{d}\bar{t}} = -1. \tag{27}$$

This equation can be solved analytically and yields

$$\bar{t}(\bar{x}) = \left(1+\frac{\xi}{2}\right)(\bar{x}_0^2 - \bar{x}^2) + \frac{1}{4}\,(\bar{x}_0^4 - \bar{x}^4) + \ln\left(\frac{\bar{x}_0}{\bar{x}}\right). \tag{28}$$

From this equation and equations (24) and (25), we calculate $\overline{\Delta P}_i$ and $\overline{\Delta P}_r$ during the collapse:

$$\overline{\Delta P}_i = \frac{2(1+\bar{x}^2)\bar{x}}{(\bar{x}^2+1)^2 + \xi\bar{x}^2}\,, \quad (\bar{t} > 0), \tag{29}$$

$$\overline{\Delta P}_r = \frac{\xi\bar{x}^2}{(1+\bar{x}^2)^2 + \xi\bar{x}^2}\,, \quad (\bar{t} > 0). \tag{30}$$

These equations allow us to plot the curves $\overline{\Delta P}_i(\bar{t})$ shown in Figure 10. These curves have been calculated

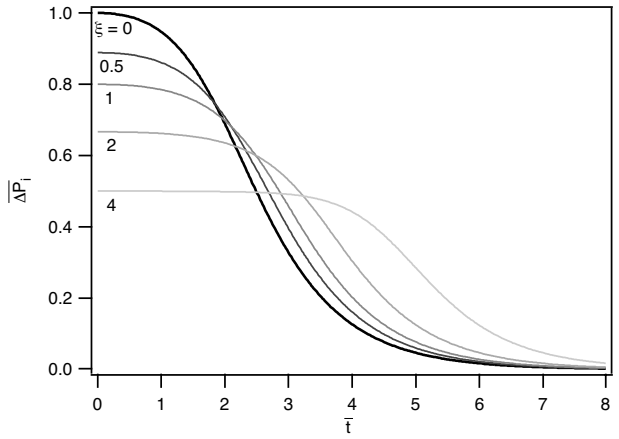

Fig. 10. Evolution of the internal pressure as a function of time. Theoretical curves calculated by assuming that $\bar{x}_0 = 1$ and $\overline{\Delta P}_i(\bar{t} = 0^-) = 1$. The value of ξ is indicated below each curve.

for different values of ξ by assuming that the bubble is initially fully inflated ($\bar{x}_0 = 1$). Their main characteristic is to present a jump $\overline{\delta P}_{i0} = \overline{\Delta P}_i(\bar{t} = 0^-) - \overline{\Delta P}_i(\bar{t} = 0^+)$ at time $\bar{t} = 0$, which increases when the ratio ξ between the smectic time and the capillary time increases. This jump is observed experimentally (although smoothed by the air compressibility effects) as can be seen in Figures 6 and 8. Note that the jump $\overline{\delta P}_{i0}$ can be easily calculated as a function of the initial height $\bar{x}_0$ of the bubble by using equations (26) and (29). Indeed, the former equation gives

$$\overline{\Delta P}_i(\bar{t} = 0^-) = \frac{2\bar{x}_0}{1 + \bar{x}_0^2} \tag{31}$$

while the latter yields

$$\overline{\Delta P}_i(\bar{t} = 0^+) = \frac{2(1 + \bar{x}_0^2)\bar{x}_0}{(1 + \bar{x}_0^2)^2 + \xi\bar{x}_0^2}\,. \tag{32}$$

From these two equations, we calculate

$$\overline{\delta P}_{i0} = \frac{2\xi\bar{x}_0^3}{(1 + \bar{x}_0^2)^3 + \xi\bar{x}_0^2(1 + \bar{x}_0^2)}\,. \tag{33}$$

Similarly, the relative pressure $\overline{\Delta P}_r$ jumps at time $t = 0$ from 0 (indeed, $\overline{\Delta P}_r(t < 0) = 0$, as the bubble is at equilibrium) to a finite positive value $\overline{\delta P}_{r0} = \overline{\Delta P}_r(t = 0^+)$ of expression

$$\overline{\delta P}_{r0} = \frac{\xi\bar{x}_0^2}{(1 + \bar{x}_0^2)^2 + \xi\bar{x}_0^2}\,. \tag{34}$$

In principle, these jumps (of maximal amplitude when $\bar{x}_0 = 1$) provide a direct measurement of ξ from which the smectic time t_{Sm} (and, consequently, the meniscus permeability C) can be deduced since the capillary time t_c is known experimentally. It turns out that the reality is more complex as will be shown in the next section.

5 Comparison with experiments: meniscus destabilization and rheological behavior of the meniscus

All the previous analysis rests on the strong assumption that the meniscus permeability C is constant during the collapse. It turns out that C has already been measured in the quasi-static regime. In the following, we shall denote by C_{qs} the corresponding value, which we recall is usually much larger than 1 and strongly dependent on the film thickness [1,6,11,12]. In the following subsection, we analyze the direct consequences of the previous theory under the assumption that $C = C_{qs}$ during the collapse. In particular, we show that the flow must rapidly destabilize the meniscus in agreement with our observations.

5.1 Meniscus destabilization

Immediately after the valve opening, the meniscus is not yet destructured and its permeability is given by C_{qs}. For a film of thickness $N > 100$, $C_{qs} \approx (N_G/N)^2$ where $N_G \approx 2700$ [12]. This result allows us to calculate the pressure increase inside the film just after the valve opening by using equations (6) and (34):

$$\Delta P_{film}(t = 0^+) = \frac{2\gamma}{H}\,\overline{\Delta P}_r(t = 0^+) = \frac{2\gamma}{Nd}\,\frac{\xi\bar{x}_0^2}{(1 + \bar{x}_0^2)^2 + \xi\bar{x}_0^2}\,. \tag{35}$$

Note we have neglected to simplify the air compressibility effects. In the quasi-static regime, ξ has for expression, according to equations (21), (18) and (19),

$$\xi_{qs} = \frac{3}{8}\,\frac{N_G^2}{N}\,\frac{da^4}{m\eta_a L r^3} \tag{36}$$

which gives explicitly $\xi = 3 \times 10^5/N$ by taking $N_G = 2700$ [12], $d = 3 \times 10^{-7}\,\mathrm{cm}$, $a = 0.04\,\mathrm{cm}$, $r = 0.5\,\mathrm{cm}$, $L = 6\,\mathrm{cm}$, $\eta_a = 1.8 \times 10^{-4}\,\mathrm{P}$ and $m = 4 \times 10^{-7}\,\mathrm{cm^2 sg^{-1}}$ [1]. As a consequence, $\xi_{qs} \gg 1$ in all our experiments and we have, according to equation (35),

$$\Delta P_{film}(t = 0^+) \approx \frac{2\gamma}{Nd} \quad \text{(in the quasi-static regime)}. \tag{37}$$

This pressure increase is considerable and is balanced by a dilation of the layers, which we know, can lead to an undulation instability of the layers rapidly followed by the nucleation of a lattice of focal parabolae. Experimentally, these defects nucleate when the dilative stress is typically larger than $10B\lambda/(Nd)$, where $\lambda = \sqrt{K/B}$ is the so-called penetration length [1,18]. In 8CB, $\lambda \approx d/3$ [1, 22], which yields a critical stress $\sigma_c \approx 3.3B/N$. In 8CB, $\gamma \approx 30\,\mathrm{dyn/cm}$ [1,23] and $B \approx 10^8\,\mathrm{erg/cm^3}$ [1,22]. We thus calculate $\Delta P_{film}(t = 0^+) \approx 2 \times 10^8/N$, while $\sigma_c \approx 3.3 \times 10^8/N$ (in $\mathrm{dyn/cm^2}$).

This simplified calculation (as it neglects air compressibility effects) shows that the film must be stable since

$\Delta P_{film}(t = 0^+) < \sigma_c$ whatever its thickness. This agrees with experiments. On the other hand, we know that the dissipation in the quasi-static regime is localized in the well-organized part of the meniscus because of the permeation flows around the dislocations [1,9,11,12]. For this reason, this region, in which the pressure drops from P_{film} down to P_m is also strongly dilated and must be unstable with respect to the formation of focal conics as long as its thickness is typically 2 times larger than the film thickness. This happens very close to the entrance of the meniscus, which, for this reason, destabilizes rapidly (within a few tens of ms) after the valve is opened. This step is well visible on the curves of Figure 6 and in Figure 7.

Another consequence of this destabilization is an abrupt decrease of the constant C from C_{qs} to a new value C_{destr} corresponding to a destructured meniscus.

In the following subsection, we show how to determine C_{destr} from the fit of the initial pressure jump.

5.2 Permeability constant of a destructured meniscus

In Figure 11 we show a set of pressure curves measured with the same film of thickness $N = 2830$ for different values of the capillary time. In this experiment, the bubble is initially expanded by half ($\bar{x}_0 = 0.5$ and $\overline{\Delta P}_i(t = 0) = 0.8$). This precaution avoids that the bubble glides on the extremity of the cylinder, which would introduce an uncertainty on r.

As expected, each curve presents a jump at the beginning which increases in size when the capillary time or, equivalently, the collapse time decreases. These jumps are smoothed by the air compressibility effects, so that the only way to fit them properly is to solve numerically the two coupled equations (24) and (25). To show the effects of the air compressibility, the curves obtained by replacing the bubble by a solid membrane were also reported: as expected, they all superpose (dashed line in Fig. 11). In addition, their fit to an exponential law gives $\kappa = 0.415$ independently of the capillary length in agreement with equations (16) and (20).

Figure 12 shows a fit of one of these experimental curves (that for which $t_c = 0.498$ s) obtained by solving numerically the two coupled equations (24) and (25). In this example, we chose the value of ξ, and so of C, in order to fit at best the initial jump. This procedure, which gives the value of C_{destr} defined in the previous subsection, was repeated for all the other curves. In Figure 13 we plotted C_{destr} as a function of the typical velocity r/t_c (which gives, in order of magnitude, the average velocity at the entrance of the meniscus). This graph shows that C_{destr} strongly decreases when r/t_c increases.

To complete these observations, we performed similar experiments with films of different thicknesses ranging typically between 500 and 3000 layers and found that, for a given capillary tube (*i.e.*, for a given value of t_c), the initial jumps were reproducible. A direct consequence is that ξ and so $C_{destr}N$ is constant (*i.e.*, independent of N). This result is important as it shows that the dissipation (measured by t_{Sm}, itself proportional to $C_{destr}N$ according to its definition (18)), is independent of N and only depends on the velocity at the entrance of the meniscus.

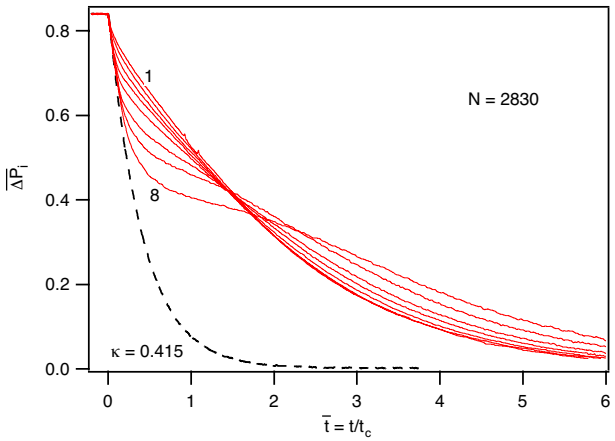

Fig. 11. Time evolution of the pressure inside the bubble. All the experiments have been performed with the same thick film ($N = 2830$). Eight curves are reported, numbered from 1 to 8. The corresponding capillary times t_c are equal, in this order, to 19.4 s, 10.7 s, 4.98 s, 1.95 s, 0.995 s, 0.498 s, 0.285 s, and 0.148 s. The shorter is t_c, the larger is the jump at the origin. The curve in dashed line (representing 8 curves superposed) has been obtained by replacing the bubble by a solid membrane. Its fit to an exponential law gives $\kappa = 0.415$.

It is also important to note that C_{destr} is always much smaller than C_{qs}, even when the collapse is slow. The reason is that the velocity at the entrance of the meniscus is always much larger than the few μm/min involved in all the previous experiments performed in the quasi-static regime.

In addition, C must increase during the collapse according to the graph of Figure 13 since the velocity at the entrance of the meniscus decreases in the same time. This remark explains why we cannot plot correctly the whole experimental curves by assuming that C is constant, equal to C_{destr} during the whole collapse.

In conclusion, a simple fit of the pressure jump is not sufficient to characterize the whole collapse, even if it already gives valuable information about the beginning of the collapse. In the next subsection, we show how to analyze the second step of the collapse dynamics (*i.e.*, after the meniscus destabilization) to determine the rheological behavior law of the meniscus.

5.3 Rheological law of the meniscus in the nonlinear regime

To determine this law, we can use our theory in its original formulation, which does not presuppose anything about the constancy of the permeability of the meniscus. Indeed, according to the general equation (6), the measurement of the shift to the Laplace law $\overline{\Delta P}_r$ allows us to determine the time evolution of ΔP_{film} during a collapse. So, plotting this quantity as a function of velocity v_m at the entrance of the meniscus, which is given by the geometrical relation $v_m = -(1/2\pi r)(\mathrm{d}S/\mathrm{d}t) = (x/r)(\mathrm{d}x/\mathrm{d}t)$, leads

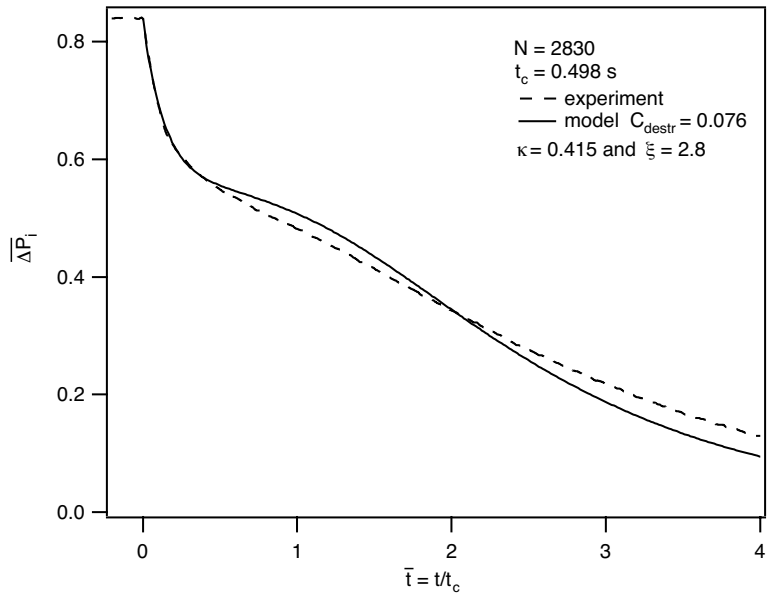

Fig. 12. Example of theoretical curve (solid line) calculated by taking $\kappa = 0.415$ which fits well the initial jump pressure. The experimental curve (dashed line) has been measured with the film of thickness $N = 2830$ and the capillary of length $L = 6\,\mathrm{cm}$ ($t_c = 0.498\,\mathrm{s}$).

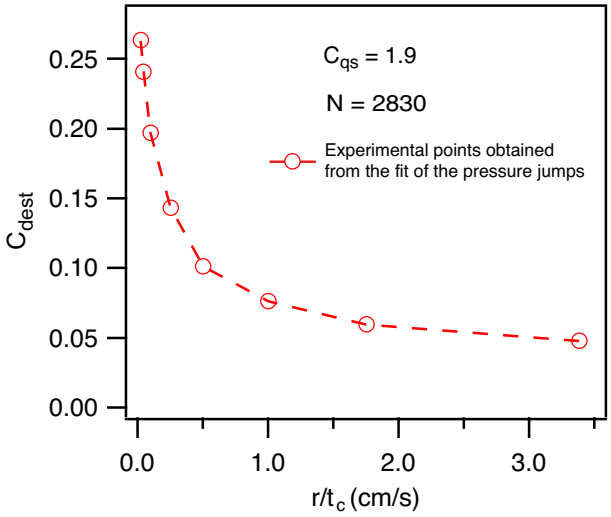

Fig. 13. Permeability C_{destr} of the destructured meniscus as a function of the typical velocity r/t_c. The value of C_{destr} was obtained by fitting the initial jumps of the experimental curves shown in Figure 11 to the theoretical model by taking $\kappa = 0.415$ and C constant. The dashed line is just a guide for the eyes.

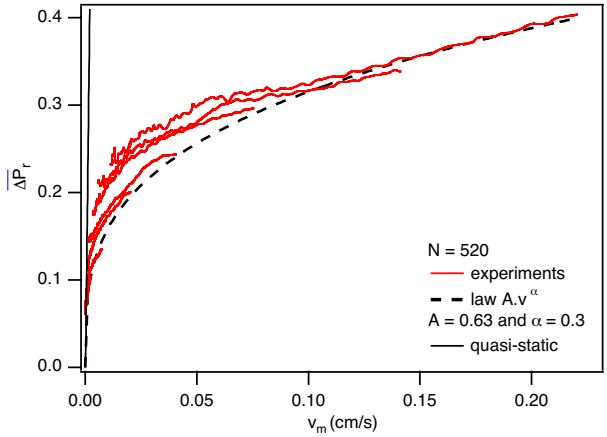

Fig. 14. Shift to the Laplace law $\overline{\Delta P}_r$ as a function of velocity v_m at the entrance of the meniscus. All measurements have been performed with the same film of thickness $N = 520$ by changing the capillary length. The dashed line corresponds to a power law of exponent $\alpha = 0.3$. The almost vertical straight line corresponds to the prediction in the quasi-static regime.

directly to the rheological law of a destructured meniscus. For each collapse experiment, $\overline{\Delta P}_r(t)$ (proportional to ΔP_{film} via Eq. (6)) and $v_m(t)$ were measured. We then plotted on the same graph all the curves $\overline{\Delta P}_r$ *vs.* v_m obtained in this way with a film of thickness $N = 520$ by changing t_c (or, equivalently, the capillary length L) (Fig. 14). As can be seen in this figure, all the curves gather into a narrow band. Although they do not exactly overlap, they all end on a well-defined single curve represented in dotted line. This curve characterizes the rheological behavior of the bubble at the beginning of the collapse, just after the meniscus destabilization. It can be fitted to a power law of type

$$\overline{\Delta P}_r = A v_m^{0.3} \tag{38}$$

with $A = 0.63$ in the present experiment. This law is very different from that we would find in the quasi-static regime, represented in full line in Figure 14. This comparison shows that the dissipation strongly decreases once the meniscus is broken. As for the meniscus, we deduce from

equation (6) that it follows the rheological law

$$\Delta P_{film} = a v_m^{0.3} \tag{39}$$

with $a = A\,\frac{2\gamma}{H}$.

We performed other experiments with films of larger thicknesses (up to $N = 2800$). In all cases, we found that the curves $\Delta P_i(t)$, $\Delta P_L(t)$, and consequently $\Delta P_r(t)$, superpose within experimental errors. As a consequence, the rheological law (38) is robust as it is independent of the film thickness (A and the exponent 0.3 are independent of N).

Nevertheless, one could be surprised by the fact that the experimental curves $\overline{\Delta P}_r(v_m)$ shift slightly (but systematically) from the previous law during the collapse. To explain this behavior qualitatively, we observed a meniscus during a slow collapse and noted its tendency to restabilize during the collapse. This restructuration makes the meniscus less permeable, whence the shift observed experimentally, in particular at the end of the collapse.

More surprising is the fact that A is a constant since, in that case, the "penetration force" of the film into the meniscus $H\Delta P_{film}$ is only a function of the velocity. This suggests that the film behaves as a solid plate penetrating into a non-Newtonian shear-thinning fluid in which it "dissolves" after a certain distance.

So far, we have only considered thick films, in which the number of layers is more than 500 typically. The situation changes in thinner films as we explain in the next section.

6 Thin films and spontaneous thickening under collapse

To complete our observations, we performed similar experiments with thin films ($N < 500$). We observed that the rheological law (38) still applies, except that, now, A decreases when the film thickness decreases. For instance, we measured $A = 0.63$ for $N = 500$, $A = 0.54$ for $N = 250$, $A = 0.45$ for $N = 180$ and $A = 0.36$ for $N = 110$. This decrease of A is a direct consequence of the experimental fact that the thinner the film is, the less it dissipates. This can be seen directly from the curves $\Delta P_r(t)$ plotted in Figure 15 for different film thicknesses, from which the preceding values of A were determined.

We could conclude from these observations that for "thin" films, the resistance of the meniscus decreases. It turns out that this explanation is certainly wrong. Indeed, systematic observations of films after the collapse reveal that islands nucleate and grow inside. As a result, the films thicken during the collapse as can be seen in Figure 16. The net result is a decrease of their resistance to the collapse as the matter can now flow both into the meniscus and the islands. Note that in this regime a (which only characterizes the rheological behavior of the meniscus) is no longer measurable. Another direct consequence of the nucleation of islands is the systematic increase of the internal pressure ΔP_i just after the initial pressure drop. This effect, which is marked by an arrow in Figure 15, increases

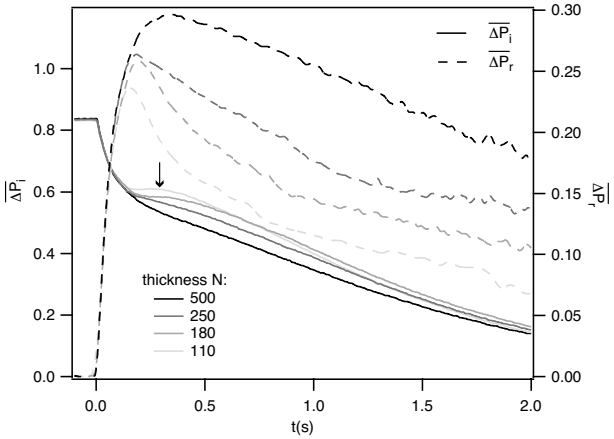

Fig. 15. Internal pressure $\Delta P_i(t)$ and shift to the Laplace law $\overline{\Delta P}_r(t)$ measured during the collapse of thin films ($100 < N < 500$). The arrow marks the pressure increase caused by the nucleation and the growth of islands. This effect increases and, thus, the smectic dissipation measured by $\overline{\Delta P}_r(t)$ decreases, when the film thickness decreases.

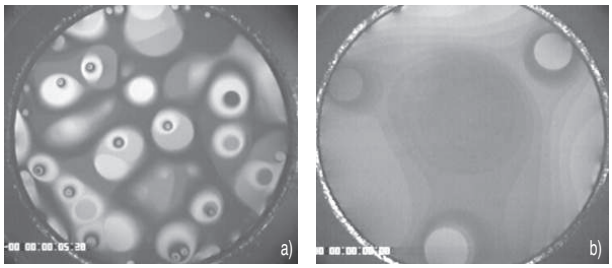

Fig. 16. Observation under the reflecting microscope in monochromatic light ($\lambda = 633\,\text{nm}$ of two thin films immediately after the bubble collapse. In a) $N = 180$ and $L = 6\,\text{cm}$. In b), $N = 110$ and $L = 192\,\text{cm}$. Even in this case of a particularly slow collapse, islands have nucleated.

when the film thickness decreases. It is associated with a new compression of the air inside the bubble just after the initial pressure drop. It is due to a decrease of the resistance of the bubble to collapse and, thus, to a decrease of the smectic dissipation caused by the island nucleation.

In order to understand why islands nucleate in thin films, let us evaluate the critical radius of nucleation r_c of a dislocation loop of Burgers vector b at the beginning of the collapse. During the meniscus destabilization, the pressure in the film increases considerably by $\Delta P_{film}(\max) = \overline{\Delta P}_r(\max)(2\gamma/H)$ (see Eq. (6)). In these conditions, the critical radius of nucleation reads

$$r_c = \frac{E_d}{b\Delta P_{film}(\max)} = \frac{E_d}{b}\,\frac{H}{2\gamma\overline{\Delta P}_r(\max)}\,, \tag{40}$$

where E_d is the dislocation energy, proportional to b [1,7]. This formula comes from the competition between the line tension which tends to collapse the island and the pressure force which tends to grow it. This formula shows also that the thinner the film, the smaller the critical radius of nucleation. For $N = 500$, this formula gives $r_c \approx 0.25\,\mu\text{m}$ by taking $E_d/b \approx 2\,\text{dyn/cm}$ [1,7,22] and $\overline{\Delta P}_r(\max) \approx 0.2$. It

can be easily checked that the associated energy barrier is still much larger than k_BT, so that homogeneous nucleation is forbidden. On the other hand, heterogeneous nucleation on dust particles of micrometric size becomes quite possible and is indeed observed.

Having understood why islands nucleate, let us now explain qualitatively why the dissipation decreases when the film thickness decreases. For this purpose, let us estimate the characteristic time t_i associated with the growth of n_i islands (experimentally, n_i is the number of nucleation centers, of the order of a few tens, see Fig. 16).

Before estimating t_i, let us show how to find again without calculation expression (18) of the smectic time t_{Sm} (obtained previously by normalizing the dynamical equation (9)). The wile is to equilibrate the surface energy gained during the collapse (assumed to be realized without capillary) with the energy dissipated, equal by definition to the product of $\Delta P_{film} = C_{destr}v_m/m$ (to simplify, we assume that $C = C_{destr}$ during the collapse) by the quantity of material which enters into the meniscus. This procedure gives

$$2\gamma\pi r^2 \sim \frac{C_{destr}v_m}{m}\,\pi r^2 N d \quad \text{with} \quad v_m \sim \frac{r}{t_{Sm}} \qquad (41)$$

from which we deduce

$$t_{Sm} = \frac{C_{destr}N dr}{2\gamma m} \qquad (42)$$

in agreement with expression (18).

Time t_i can be obtained by reasoning in a similar way. Now, we assume that there is no capillary and no exchange of matter with the meniscus. In other words, we assume that the filling of the islands which have nucleated at the beginning of the collapse is the only source of dissipation. Equaling the gain of surface energy with the dissipated energy yields

$$2\gamma\pi r^2 \sim n_i \frac{v_i}{\left(\frac{N}{N+k}\right)m}\,\pi r_i^2 k d \quad \text{with} \quad v_i \sim \frac{r_i}{t_i}\,. \qquad (43)$$

In this equation, n_i is the number of islands, k is the Burgers vector of each dislocation (in number of layers, $b = kd$), v_i is the typical growth velocity of an island and $v_i/[m(N/N + k)]$ is the pressure difference between the film and the islands when they fill (knowing that the mobility of a dislocation in a film is equal to $mN/(N + k)$ as was shown in Ref. [1]). In addition, the mass must be conserved, which imposes $n_i k r_i^2 = Nr^2$. From these two equations, we calculate

$$t_i(n_i, k) = \sqrt{\frac{N}{n_i k}}\,\frac{(N+k)dr}{2\gamma m}\,. \qquad (44)$$

This relaxation time is inversely proportional to the number of islands. It also passes through a minimum when the Burgers vector of the dislocations is equal to the film thickness: $k = N$. In this case, the dissipation is minimal and time t_i reads

$$t_i(n_i) = \frac{1}{\sqrt{n_i}}\,\frac{Ndr}{\gamma m}\,. \qquad (45)$$

We can now compare the two processes. Experiments have shown that $C_{destr}N$ which characterizes the dissipation due to the flow of material into the meniscus is constant in thick films. Because there is no reason for this result to be wrong in thin films, we will assume it holds whatever the film thickness. The direct consequence is that t_{Sm} is independent of N whereas t_i is proportional to N. It turns out that the collapse time is fixed by the shortest time as it corresponds to the less dissipative process. For this reason, we predict that the collapse will be dominated by the nucleation and the growth of islands in thin films, and by the exchange of material with the meniscus in thick films.

In practice, the crossover between the two regimes is given by equaling these two times. That gives the typical film thickness: $N(\text{crossover}) \sim NC_{destr}\sqrt{n_i}$. In experiments with the capillary of length $L = 6\,\text{cm}$, $NC_{destr} \approx 2830 \times 0.05 \approx 150$ (see Fig. 13), which gives by taking $n_i \sim 10$, $N(\text{crossover}) \sim 500$. This value agrees with experiments.

7 Conclusions

We have shown that a smectic bubble inflated at the end of a capillary tube can collapse while keeping a constant film thickness provided that the film is thick enough. In this case, the dynamics is only governed by the flow of material at the entrance of the meniscus. We have shown that this process is well characterized from a rheological point of view when the lamellar structure in the meniscus is completely destructured. This destructuration takes place at the very beginning of the collapse and is caused by the nucleation of focal conics within the well-oriented part of the meniscus where the pressure strongly increases. Once the meniscus is destabilized, the pressure difference between the film and the meniscus is proportional to the velocity of the material at the entrance of the meniscus to the power 0.3, with a proportionality constant independent of the film thickness. This highly nonlinear rheological law was determined directly by measuring simultaneously the pressure inside the bubble and the Laplace pressure. It strongly differs from the linear law found in the quasi-static regime at very small velocities. It must be stressed that the dissipation is much smaller in this regime than it would be if the linear law found in the quasi-static regime was applicable.

In thin films the situation becomes more complicated because islands can easily nucleate in the film. The reason is that their critical radius of nucleation is proportional to the film thickness. So, for a thinner film the nucleation of islands on dust particles becomes easier. In addition, the film can now exchange material with both the islands and the meniscus. For these two reasons, the thinner the film is, the faster the bubble collapses.

It is important to note that the method developed in this paper consisting of measuring the shift to the Laplace law is very powerful as it gives directly the time evolution of the global dissipation inside the bubble, whatever its

physical origin, providing that inertial effects can be neglected. This method is also generic because it can be applied to other systems such as soap films or polymeric films for which the different sources of dissipation are not yet clearly identified. For that reason, we started to study the deformations of soap bubbles in which preliminary measurements have already shown visible effects. The next step will be to extend these experiments to more complex geometries. One of them, which we have already analyzed in the static regime consists of a catenoid truncated by a planar film [24]. This structure is interesting because it resembles an elementary cell in a foam. Observing its deformation under pressure variation could thus be very useful to address the general problem of the dissipation in foams.

References

1. P. Oswald, P. Pieranski, *Smectic and Columnar Liquid Crystals*, in the *Liquid Crystals Book Series* (Taylor & Francis, Boca Raton, 2005) Chapt. 8.
2. F. Picano, P. Oswald, E. Kats, Phys. Rev. E **63**, 021705 (2001).
3. P. Pieranski, L. Beliard, J.-Ph. Tournellec *et al.*, Physica A **194**, 364 (1993).
4. E.A.L. Mol, G.C.L. Wong, J.M. Petit, F. Rieutord, W.H. de Jeu, Physica B **248**, 191 (1998).
5. T. Stoebe, P. Mach, C.C. Huang, Phys. Rev. Lett. **73**, 1384 (1994).
6. P. Oswald, *Thinning transitions in free-standing smectic A films* in *Phase transition. Application to Liquid Crystals, Organic Electronic and Optoelectronic Fields*, edited by Vlad Popa-Nita (Research Signpost, Kerala, India, 2006).
7. J.-C. Géminard, R. Holyst, P. Oswald, Phys. Rev. Lett. **73**, 1384 (1994).
8. S. Pankratz, P.M. Johnson, R. Hoylst, C.C. Huang, Phys. Rev. E **60**, R2456 (1999).
9. P. Oswald, P. Pieranski, F. Picano, R. Holyst, Phys. Rev. Lett. **88**, 015503 (2002).
10. F. Picano, R. Holyst, P. Oswald, Phys. Rev. E **62**, 3747 (2000).
11. P. Oswald, F. Picano, F. Caillier, Phys. Rev. E **68**, 061701 (2003).
12. F. Caillier, P. Oswald, Phys. Rev. E **70**, 031704 (2004).
13. P. Oswald, J. Phys. (Paris) **48**, 897 (1987).
14. R. Stannarius, C. Cramer, Liq. Cryst. **23**, 371 (1997)
15. R. Stannarius, C. Cramer, Europhys. Lett. **42**, 43 (1998)
16. H. Shüring, C. Thieme, R. Stannarius, Liq. Cryst. **28**, 241 (2001).
17. Note that this condition was not fulfilled in the experiment performed in 1987 [13]. We think today that several concentric pores were present in the film before the bubble started to collapse (a photograph of such a pore in a bubble is shown in Ref. [14]). As a consequence, the dissipation was certainly due in this experiment to the pore closing and, to some extent, an exchange of matter with the meniscus.
18. Ch.S. Rosenblatt, R. Pindak, N.A. Clark, R.B. Meyer, J. Phys. (Paris) **38**, 1105 (1977).
19. R.B. Bird, W.E. Stewart, E.N. Lightfoot, *Transport Phenomena* (Wiley, New York, 1960).
20. F. Caillier, *Dynamique des dislocations coin et dissipation dans les films librement suspendus de cristal liquide smectique*, PhD Thesis, Ecole Normale Supérieure de Lyon, 2005.
21. D.J. Tritton, *Physical Fluid Dynamics* (Van Nostrand Reinhold, Cambridge, 1977).
22. A. Zywocinski, F. Picano, P. Oswald, J.-C. Géminard, Phys. Rev. E **62**, 8133 (2000).
23. R. Jacquet, F. Schneider, Phys. Rev. E **67**, 021707 (2003).
24. J.-C. Géminard, A. Zywocinski, F. Caillier, P. Oswald, Philos. Mag. Lett. **84**, 199 (2004).